

S. Werner<sup>1</sup>, Z. Velinov<sup>1</sup>, W. Jakob<sup>2</sup> and M. B. Hullin<sup>1</sup>
<sup>1</sup>Rheinische Friedrich-Wilhelms-Universität Bonn, Germany <sup>2</sup>EPFL

## Abstract

This supplemental material provides detailed derivations and parameters for recreation of results presented in the main body of our paper. In particular, we show a detailed derivation of the BRDF from Harveys *diffracted radiance* on which our model is based. Additionally, we list all render settings and scratch parameters and the corresponding render times for all results obtained with our model.

## 1 Diffracted radiance

Our model builds on tools from Fourier optics [1], specifically the *angular spectrum* and the concept of *diffracted radiance* [2], which we review here for completeness. Being part of a *scalar* theory of light transport, these two tools assume that the electromagnetic field can be described by the (scalar) amplitude of the oscillations that make up the electromagnetic field, as opposed to the commonly used vectorial electric and magnetic fields. This approximation is accurate in the far-field and for diffracting apertures that are larger than the wavelength of the radiation. Without loss of generality, we restrict ourselves to monochromatic radiation at a wavelength of  $\lambda$ . The following discussion assumes that all spatial coordinates are expressed in units of  $\lambda$ , since this leads to simpler mathematical expressions. Let  $U(x, y, z)$  denote the scalar amplitude at position  $(x, y, z)^T$ , and let  $U_0(x, y) := U(x, y, 0)$  denote a planar slice at position  $z = 0$  (here called the aperture plane). A well-studied problem in this domain entails computing  $U(x, y, z)$  for  $z > 0$  given the amplitude distribution in the aperture plane  $U_0(x, y)$ . In the context of Fourier optics, solutions can be found by taking the Fourier transform of all quantities in the  $xy$ -plane, i.e.

$$V(\alpha, \beta, z) := \mathcal{F}\{U(\cdot, \cdot, z)\}_{\alpha, \beta}, \quad V_0(\alpha, \beta) := \mathcal{F}\{U_0(\cdot, \cdot)\}_{\alpha, \beta}, \quad (32)$$

and solving the Helmholtz equation  $[\nabla^2 + 4\pi^2]U = 0$  analytically in terms of the frequency-space representation  $V$ . The latter has an intuitive physical interpretation: the amplitude  $U(x, y, z)$  on any fixed  $z$ -slice can be described as a superposition of plane waves arriving from different directions. In this context,  $V(\alpha, \beta, z) \in \mathbb{C}$  denotes both phase and amplitude of such a plane wave arriving from direction  $(\alpha, \beta, \gamma)$  where  $\gamma = \sqrt{1 - \alpha^2 - \beta^2}$  (Figure 3a, main paper). The variables of this parameterization are referred to as *direction cosines*. Evaluating the superposition of plane waves is equivalent to an inverse Fourier transform that recovers the original signal. Assuming that radiation travels undisturbed through the half-space  $z > 0$ , the Helmholtz equation has a particularly simple solution which states that the plane waves arriving at any  $z$ -slice correspond exactly to those at  $z = 0$  except for a phase shift  $V(\alpha, \beta, z) = V_0(\alpha, \beta)e^{i2\pi\gamma z}$ . This solution is exact under the stated assumptions, but the resulting field  $U(x, y, z)$  is prohibitively expensive to evaluate due to its definition in terms of a pair of Fourier transforms. We instead rely on a far-field approximation, which makes the reasonable assumption that the distance between the surface and the camera is much greater than the wavelength of light (Figure 3a and Figure 4(d), main paper). This far-field approximation, known as *diffracted radiance*, was introduced by Harvey et al. [2] and is

defined as

$$L(\boldsymbol{\omega}) = \frac{\lambda^2}{A_s} |\mathcal{F}\{U_0(\cdot, \cdot)\}_{\alpha, \beta}|^2 = \frac{\lambda^2}{A_s} |V_0(\alpha, \beta)|^2, \quad (33)$$

where  $\boldsymbol{\omega} = (\alpha, \beta, \gamma)$ .  $U_0$  describes both the source for the field at  $z > 0$  and the result of the radiation incident at  $z = 0$ , as the corresponding angular spectrum  $V_0(\alpha, \beta)$  is given by the superposition of plane waves from all directions. A change of the direction of incident radiance by direction cosine  $\beta_i$  results in a shift applied to all plane waves contributing to  $V_0(\alpha, \beta)$ , and the angle-shifted angular spectrum now reads  $V_0(\alpha, \beta - \beta_i)$  (we show the one-dimensional case for simplicity, but the concept holds for the second dimension as well). As angular spectrum and complex amplitude are related by a Fourier transform, this can be interpreted in terms of the Fourier shift theorem as a linear phase shift applied to  $U_0$ . An additional attenuation factor, the third direction cosine  $\gamma_i$  [2], accounts for the decreased intensity at oblique incident angles and modulates Eq. 33 as

$$\begin{aligned} L(\boldsymbol{\omega}, \alpha_i, \beta_i) &= \gamma_i \frac{\lambda^2}{A_s} |V_0(\alpha - \alpha_i, \beta - \beta_i)|^2 \\ &= \gamma_i \frac{\lambda^2}{A_s} |\mathcal{F}\{U_0(\cdot, \cdot) e^{2\pi i(\beta_i y + \alpha_i x)}\}_{\alpha, \beta}|^2. \end{aligned} \quad (34)$$

This influence of the angular distance in direction cosine space on the diffracted radiance is also known as *shift invariance*.

## BRDF model

Following Sec.3.2 (main paper) we repeat the well-known definition of the bidirectional reflectance distribution function (BRDF) and the accompanying notations for completeness;

$$f_r = \frac{dL_s(\boldsymbol{x}, \hat{\boldsymbol{\omega}}_o)}{dE_i(\hat{\boldsymbol{\omega}}_i)}, \quad (35)$$

which relates differential irradiance to scattered radiance.  $\boldsymbol{x}$  represents a position on the surface,  $\hat{\boldsymbol{\omega}}_i$  is the direction from which this surface is illuminated and  $\hat{\boldsymbol{\omega}}_o$  the direction from which it is observed. The radiance scattered by a diffracting aperture is given by Eq. 34 as a function in direction-cosine space using a coordinate system where all spatial variables are normalized to the optical wavelength. A change of variables enables us to rewrite the representation of the Fourier transform in a non-scaled coordinate system as

$$L_s(\boldsymbol{\xi}) = \gamma_i \frac{1}{A_s} \frac{1}{\lambda^2} |\mathcal{F}\{U_0(\boldsymbol{x})\}_{\xi_{1,2}}|^2 \quad (36)$$

We can describe the complex wavefront  $U_0(\boldsymbol{x})$  in the surface plane by the modulation of the wavefront of the incident light  $U_i(\boldsymbol{x})$  with the so-called *transfer function*  $\mathcal{T}(\boldsymbol{x})$  [3, 1] of the diffracting plane as

$$U_0(\boldsymbol{x}) = U_i(\boldsymbol{x}) \cdot \mathcal{T}(\boldsymbol{x}). \quad (37)$$

Since the diffracting aperture is uniformly illuminated ([2]), we can neglect the position dependence of the complex amplitude of the incident light in the aperture plane. Thus,  $U_i(\boldsymbol{x}) = U_i$  is a constant modulation factor. Substitution into Eq. 36 then yields

$$L_s(\boldsymbol{\xi}) = \gamma_i \frac{1}{A_s} \frac{1}{\lambda^2} |U_i|^2 |\mathcal{F}\{\mathcal{T}(\boldsymbol{x})\}_{\xi_{1,2}}|^2. \quad (38)$$

In the context of a BRDF definition,  $U_i$  corresponds to the differential incident radiance, i.e.  $E_i = |U_i|^2$ , which enables us to substitute Eq. 38 into Eq. 35; we can therefore write

$$f_r(\boldsymbol{\xi}) = \gamma_i \frac{1}{A_s} \frac{1}{\lambda^2} |\mathcal{F}\{\mathcal{T}(\mathbf{x})\}_{\boldsymbol{\xi}_{1,2}}|^2. \quad (39)$$

## References

- [1] J. Goodman. *Introduction to Fourier Optics*. McGraw-Hill Series in Electrical and Computer Engineering: Communications and Signal Processing. McGraw-Hill, 1996.
- [2] J. E. Harvey, C. L. Vernold, A. Krywonos, and P. L. Thompson. Diffracted radiance: a fundamental quantity in nonparaxial scalar diffraction theory: errata. *Appl. Opt.*, 39(34):6374–6375, Dec 2000.
- [3] A. Lipson, S. G. Lipson, and H. Lipson. *Optical physics*. Cambridge University Press, Leiden, 2010.
- [4] J. Stam. Diffraction shaders. In *Proceedings of the 26th Annual Conference on Computer Graphics and Interactive Techniques*, SIGGRAPH '99, pages 101–110, New York, NY, USA, 1999. ACM Press/Addison-Wesley Publishing Co.

Figure	$N_\lambda$	Scene	Scratch count	Scratch parameters	Variation parameters	Render time [min]
Fig. 1 (middle)	16	Dining table	300000	$U_D[0, 6]\mu m; U_W[0, 6]\mu m$	–	93
Fig. 1 (insert)						197
Fig. 1 (right)	16	Door	370000	$U_D[0, 6]\mu m; U_W[0, 6]\mu m$	–	32
Fig. 1 (insert)						67
Fig. 6 (top, left)	16	Door	370000	$U_D[0, 6]\mu m; U_W[0, 6]\mu m$	$D[1.1, 0.04]$	33
Fig. 6 (top, middle)	16	Dining table	300000	$U_D[0, 6]\mu m; U_W[0, 6]\mu m$	$D[1.1, 0.04]$	120
Fig. 6 (insert)						147
Fig. 6 (top, right)	16	CD	3128400	$D = 120nm; W = 1\mu m$		1029
Fig. 6 (bottom, left)	16	Spoon	100000	$U_D[0, 6]\mu m; U_W[0, 6]\mu m$	$D[1.1, 0.04]$	69
Fig. 6 (bottom, middle)	16					83
Fig. 6 (bottom, right)	16					368
Fig. 7 (b, @1MP)	16	Plate	3000	$G_D[250, 80]nm; G_W[4, 1.3]\mu m$	$D[1.1, 0.04]$	15
Fig. 7 (d)	16	Disc	3700	$G_D[250, 80]nm; G_W[5, 1.6]\mu m$	$D[1.1, 0.03]$	25
Fig. 8 (b)	16	CD	BRDF*	BRDF*	–	200
Fig. 8 (d)	16	CD	BRDF*	BRDF*	–	204
Fig. 9 (left, incoherent)	16	Grated plate	1600	$D = 1\mu m; W = 1\mu m$	–	14
Fig. 9 (right, coherent)						19
Fig. 10 (a)	16	Scratched plate	1500	$D = 250nm; W = 1\mu m$	$D[1.1, 0.04]$	32
Fig. 10 (b, specular)						23
Fig. 10 (c, diffuse)						23
Fig. 11 (a)	16	Dining table	300000	$U_D[0, 6]\mu m; U_W[0, 6]\mu m$	–	266
Fig. 11 (b)					$D[1.1, 0.04]$	284
Fig. 11 (c)					–	167
Fig. 11 (d)					$D[1.1, 0.04]$	168
Fig. 12 (left, @1MP)	3	Ring	547381	$D = 500nm; W = 1\mu m$	–	23
Fig. 12 (right, @1MP)	3	Plate	481905	$G_{D,W}[4.0, 0.01]\mu m$		31
Fig. 17:SuppMat (left)	16	Plate	3000	$D = 1\mu m; W = 2\mu m$	$D[1.1, 0.03]$	30
Fig. 17:SuppMat (right)	16	Plate	3000	$D = 1\mu m; W = 2\mu m$	$D[1.1, 0.03]$	31

Performance values, scratch parameters and render settings for the renderings presented. Rendering was performed on 72 CPU cores (i7-5820K@3.30GHz) and, if not stated otherwise, corresponds to a resolution of 4MP@16384 samples per pixel(SPP). The high number of SPP results from the fact that we rely on Monte Carlo integration over the pixel footprint, which is inherently done by the ray-tracer, to achieve incoherent superposition of the coherent subsamples responsible for diffraction and interference. All scenes except Figures 7, 8, 9 and 10 were scratched using our editing tool.

$N_\lambda$  gives the number of spectral samples used, the total number of scratches within the scene is given by scratch count.

Scratch parameters describes the parameters used to generate the scratch profiles on the surface, namely width and depth.  $U[lower, upper]$  refers to a uniform,  $G[mean, stddev]$  to a Gaussian distribution from which these parameters are drawn and the respective parameter is denoted via the index  $W$  for width and  $D$  for depth. For constant parameters the notation reads  $index = value$ .

Variation parameters are given as a tuple  $[amplitude, frequency]$  describing the relative variation amplitude and frequency of the respective parameter. The frequency thereby is based on a simplex-noise function with 255 gradients, such that a frequency of  $1/255$  corresponds to exactly one oscillation along the scratch. Notation for the respective parameter is given by the prefix  $W[\dots]$  for width and  $D[\dots]$  for depth.

Render time is given in minutes and is always set to the next larger integer value.

BRDF\* relates to a CD-BRDF generated for periodic surfaces. We created an ensemble of parallel scratches within one circular coherent sample, their parameters depth and width as well as their separation are taken from Stam [4]. Only view- and lighting conditions change within the rendering, the ensemble itself is constant. For the parameters taken from Stam, the number of scratches within the coherence area, and thus every coherent subsample, is  $n = 2 \frac{3\sigma}{\Delta_{\text{track}} + W_{\text{scratch}}} + 1 \approx 21$ , where  $\Delta_{\text{track}}$  is the track separation,  $W_{\text{scratch}}$  the scratch width and  $\sigma = \delta_c/6$  the standard deviation of the Gaussian filter kernel.

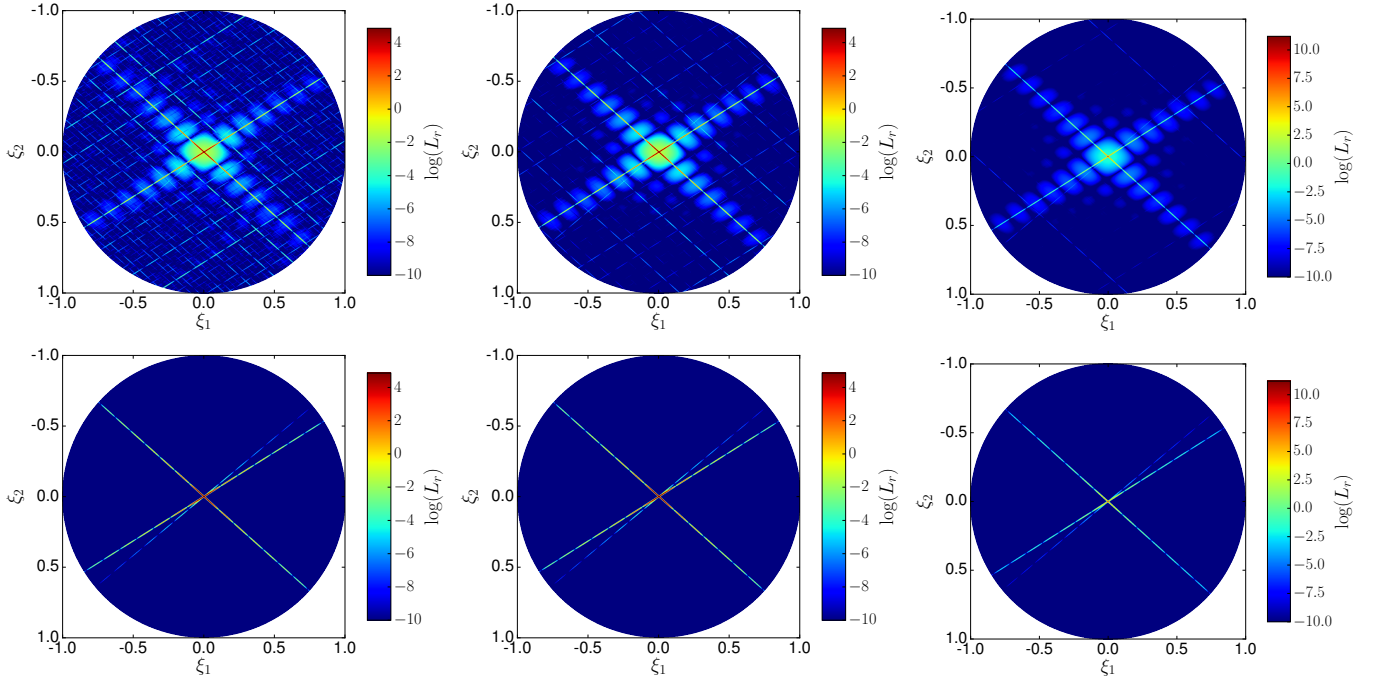


Figure 15: Comparison of radiance reflected of a scratched surface. The numerical solution (left) was computed using an explicit heightmap (c.f. Fig. 16), the analytical solution (right) was obtained using our model. The ghosting artefacts due to discretization are suppressed with increasing resolution of the heightmap whereas the parallelogram-shaped features originating from scratch-scratch intersections are not reproduced by our model. The (square) heightmaps are supplied with resolutions of 9 MP (upper row), 36 MP (middle row) and 144 MP (bottom row) with an area of  $1 \text{ mm}^2$ . This figure supplements Sec. 6:Approximation evaluation.

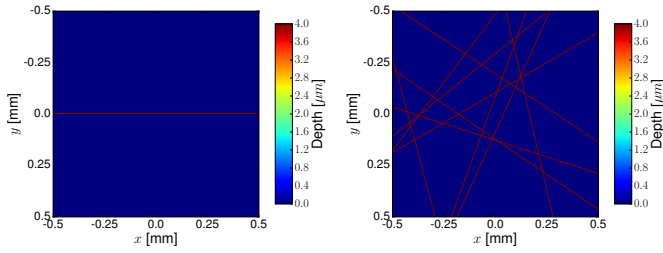


Figure 16: Surface heightmaps used as input for the numerical computation of reflected radiance for a single scratch (left) and ten randomly distributed scratches (right). This figure supplements Sec. 6:Approximation evaluation.

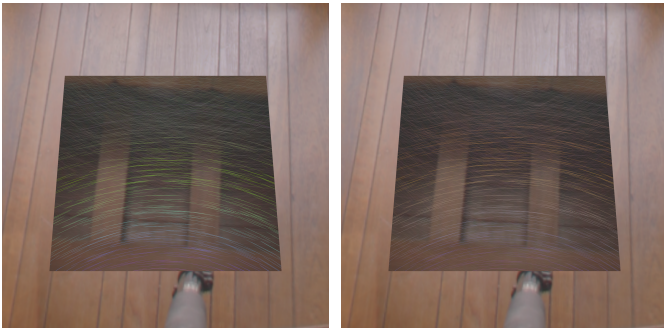


Figure 17: Rendering of a scratched plate with 3000 scratches uniformly distributed on the surface. Scratch parameters (depth, width) are kept constant, only the profile is changed from rectangular (left) to triangular (right). The change of the scratch profile results in a different scratch response function and thus reflectance distribution visible as a change in color of the scratches. This figure supplements Sec. 7:Other scratch profiles.